Chapter 7

Outer Rotor SRM Design for Electric Vehicle without Reducer via Speed-Up Evolutionary Algorithm

Zeki Omaç, Mehmet Polat, Mustafa Kaya, Eyyüp Öksüztepe, Haluk Eren, Merve Yıldırım and Hasan Kürüm

Additional information is available at the end of the chapter

http://dx.doi.org/10.5772/intechopen.74451

Abstract

Reducers utilized in automotive industry provide motor to run in most effective region and transmission output torque to increase. However, they cause mass and cost to increase and also efficiency to decrease due to mechanical losses. The aim of this study is to design a direct drive motor (outer rotor switched reluctance motor (OR-SRM)) without reducer resulting in enhanced efficiency for electric vehicle (EV). To estimate dimension and electrical parameters of OR-SRM, mathematical equations are originally derived from its geometry. Considering the constraints of package size and outer diameter, all the dimension parameters of the motor are optimized via multi-objective genetic algorithm (MOGA) to get the desired efficiency and torque. In order to validate the results in the proposed approach, OR-SRM is modeled by Maxwell 3D using optimized dimension parameters. In-wheel OR-SRM with 18/12 poles (30 kW) is manufactured to employ it in an EV. Theoretical results are compared to experimental results. It can be concluded that the results are satisfactory.

Keywords: outer rotor SRM design, nonreducer, electric vehicle, multi-objective genetic algorithm optimization

1. Introduction

Nonreducer structure of the direct drive systems provides avoiding extra mass and cost. They also enable to enhance energy efficiency due to decreasing mechanical losses. It is still a matter of debate how much benefit we can get with in-wheel motors. From a research perspective, authorities are very optimistic, but, economically, it does not make sense for commercial

vehicles right now. Coordinating the in-wheel motors requires complex control systems, and it is not so hard to foresee that in-wheel technology takes not too long to be competitive.

Developers deserve to design motors with simple structure, high power density, and low cost. Permanent magnet synchronous motors (PMSMs) match aforementioned requirements, and they have been commonly employed in commercial EVs. PMSMs are widely employed in EVs due to their high power density and efficiency. Another motor type used in EVs is PM-assisted SynRM motors. They have important advantages such as low rotor losses, high saliency ratio (Lq/Ld), high torque, and high power factor. Furthermore, brushless DC motors are used in EVs due to having high torque at low speed and a proper torque-speed characteristic [1]. However, there are some drawbacks for these three motor types. The centrifugal force in the motor causes the stress in the rotor. This stress should be calculated and minimized by design optimizations [2, 3]. Besides, the magnets may be demagnetized due to reverse magnetic field and high temperature. They also cause uncontrollable regenerative operation owing to constant magnet flux existence. And also, magnet cost is considerable. SRMs are employed by various application areas such as aircrafts, EVs, marine propulsion systems, linear drives, mining drives, handheld tools, home utilities, etc. because of its inherent modularity and fault tolerance [4]. The motor behavior does not depend on the temperature due to not having the magnets [5]. There are many advantages of SRMs for EV such as not having brush, collector, magnets, and rotor consisting of only silicone sheets. It results in low production cost [6]. There is less maintenance requirement than the other electric machines. Not having magnet provides the motor to be operated at high speed. Rotor copper losses do not exist due to none rotor winding. Therefore, rotor temperature is lower than that of other motor types, and motor can be easily cooled. Low inertia is significant in variable reference speed applications to get fast response for reference speed. The rotor of SRM has also lower inertia than the other motors, and the efficiency of SRM is over 95% [7]. Once one of the phases fails, the motor continues to operate due to not any connection between the phases [8]. That property makes it a very preferable choice for aircraft applications [9]. Conversely, SRM needs both a motor driver and a rotor position sensor [1, 10]. On the account of all features, it is seen that SRM is a proper motor type for EV applications and it may become promising for the near future.

In this study, we have investigated OR-SRM with outer rotor structure unlike conventional SRMs. In-wheel SRM is more preferable due to losses and weight of driveline rather non-in-wheel scheme. In spite of increasing the system complexity, coordinating each motor enables numerous advantages with regard to safety and efficiency. For example, the drive structure of the car could be flexibly reorganized in front, rear, or four-wheel considering the road conditions.

1.1. Problem statement

The essential forces influencing movement of a vehicle are in three folds, which are a force causing gravity as climbing up a ramp with specified slope, aerodynamic force varying with square of vehicle velocity, and required force of a vehicle having specified mass to accelerate. These are vehicle dynamics employed in this study. A motor for an EV should be designed

http://dx.doi.org/10.5772/intechopen.74451

both to directly (nonreducer) generate a torque satisfying aforementioned forces and to have a size fitting specified tire. A motor having adequately small size to fit in a tire needs high currents to keep generating a continuous high torque. High-efficient electric motor should be designed to increase the range of EV.

Electric motor losses including copper, friction, windage, and iron losses play an important role in energy efficiency. Energy efficiency is directly proportional to the range, which affects the range of EV. Predominantly, one of the losses is copper losses. To reduce these, battery voltage is increased and/or winding resistance is decreased. When battery voltage is increased for a motor having same power, the current reduces. Therefore, the copper losses will decrease. However, increasing battery voltage is restricted due to motor driver and personal safety. Winding resistance can be reduced as conductor cross section is enlarged. It may not be possible to use a very large conductor cross section residing in the motor both having a size to fit in a tire and generating required torque. Thus, a maximum conductor cross section for winding should be selected such that it can fit in splines of the motor.

The torque of SRM is directly proportional to both square of the motor current and derivative of the motor phase inductance with respect to rotor position. Variation of motor phase inductance depends on dimension parameters of the motor. Therefore, these parameters should be optimized to maximize torque and efficiency of the motor. The parameters of OR-SRM consist of stator-rotor pole arc angles and pole heights, inner and outer yoke lengths, and outer diameter of the stator. Optimization of parameters using conventional or linear methods takes long time, or it might be impossible, since solution space expands as the number of parameters to optimize increases. When the dimension parameters of the OR-SRM are optimized, magnetic circuit equations should be formulized to decide whether objective function is feasible for dimension parameters. As a motor is constructed with the mentioned design considerations, problem statement can be provided in brief as follows:

- How can a motor be designed such that its torque should directly satisfy the forces on a vehicle having a weight of nearly 2 tons and also it should have a dimension to fit the tire?
- While a motor having specified constraints generates required high torque, how the heat dissipation problem could be solved?
- How should an efficient motor be designed to increase range of the car?
- There are a lot of dimension parameters effecting efficiency and torque of the reluctance motor. Which parameters can be optimized?
- How the magnetic circuit equations associated with the dimension parameters of OR-SRM can be derived to employ them in the optimization problem?

1.2. Related work

Designing a high torque motor is deserved for direct traction EVs. Thus, diameter and package length of the machine should be configured such that designed motor can fit into each wheel. Relation between torque and dimensions including diameter and length of SRM was explained

in detail [11–13]. In a research on designing SRM [14], the design and analysis with FEM of SRMs were studied, and the motor characteristics such as flux density, torque, current, and inductance values were investigated. Another paper presented a design, analytical verification, implementation, and testing of a 250 W, 200 rpm, 36 V, 15 Nm SR hub motor. Infolytica Magnet 6.24.1 software was used for verifying winding inductance and torque. According to the authors, the proposed motor with exterior motor structure could be easily incorporated within the wheels of a low-cost, low-weight EV [15]. In [16, 17], theoretical calculations of SRM and numerical analysis by 2D FEM were carried out. Also, dynamic behavior of a 12/8 SRM and the effect of motor characteristics were investigated. In [18], design and analysis of a SRM for next-generation hybrid vehicle without PM materials were realized. Maximum torque and efficiency of SRM were investigated for 6/4, 8/6, 12/8, and 18/12 SRMs as varying stator taper angles. Authors in [19] investigated a prototype machine of a SRM with respect to an IPMSM in a HEV, in terms of torque density, efficiency, and torque-speed range. Static and light load tests were realized for these machines. The authors in [20] presented a novel multi-objective optimization method based on a genetic fuzzy algorithm. Optimum design of SRM was obtained by this method in terms of two objective functions, which are high efficiency and low torque ripple. Optimum design approach for a two-phase SRM drive via genetic algorithm (GA) was proposed in [21]. Three GA loops work to optimize the lamination design and to meet the requirements for the target application while simultaneously fine-tuning the control parameters. A dynamic simulator based on an analytical expression of magnetizing curves and a geometric flux-tube-based nonlinear magnetic analysis was developed specifically for this class of motor. The experimental results of two-phase 8/6 prototype manufactured were validated with the optimized design. 8/6 SRM was designed by Taguchi optimization method for applications requiring fast actuation [22]. This was accomplished by two simultaneous optimizations of SRM which were optimization of motor torque and the torque per rotor inertia. Two orthogonal arrays (OA) were used for leading the design of experiments (DOE), and FEA was used for computing the performance of the motor designs generated by the Taguchi DOE. Authors claimed that this method provided a high electromagnetic torque to inertia ratio required for high rates of mechanical acceleration and robustness. Analysis and nonlinear optimization of four phases 8/14 SRM were accomplished by a combination of MATLAB and 2D FEM Software Ansoft Maxwell [23]. Here, torque ripple was minimized; all the factors including torque, torque quality, torque density, and losses were maximized by using GA. Reference [24] suggested an optimization method based on GA for an efficient design of a SRM. Some parameters such as stator and rotor pole arc, rotor diameter, and stack length were determined in this paper. Magnetic field analysis was done using FEA-based CAD package, and optimum results were obtained by GA. MOGA function including efficiency and torque ripple is presented to obtain optimum design parameters that are turn-on and turn-off angles and limited current in switching elements [25]. Improved magnetic equivalent circuit (IMEC) method was used to predict the performance of SRM and to generate the input–output data. Hence, the optimal fuzzy rules were determined. M.C. Costa and his colleagues realized optimization of 4/6 SRM to estimate the most significant parameters maximizing the magnetic torque of the motor and diffuse elements response surface [26]. The diffuse element method was also used to build a response surface representing an approximation of the real objective function. This study provided reduction of optimization parameters, reducing the computation

http://dx.doi.org/10.5772/intechopen.74451

time and increasing of the magnetic torque. In another paper, optimum design of pole shapes of SRM with three-phase 6/4 pole was accomplished by ordinary kriging model and GA to minimize torque ripple [27]. As the kriging model with the uniform sampling was used to construct a response surface, GA finds an optimal point of the approximate objective function. The proposed method was verified with high computation efficiency in terms of reducing the torque ripple. Cong Ma and his friends [28] presented multi-objective optimization of SRM based on a combination of DOE and particle swarm optimization. Maximizing torque per active mass and efficiency and minimizing torque ripple were provided by this method. Authors in [29] carried out the design and analysis of an in-wheel OR-SRM with 8/6 poles for electric bus applications. Derivation of the output power equation as a function of the motor dimensions and parameters was handled. The results of the developed machine obtained by FEA were compared with that of a conventional SRM. In this study, torque ripple decreased and motor efficiency considerably increased. Multi-objective optimization design of in-wheel SRMs in EV was realized in [30]. An optimization function was developed to maximize average torque, average torque per copper loss, and average torque per motor lamination volume. The stator and rotor pole arc angles were taken as the optimized variables. A prototype of the optimally designed in-wheel SRM for EVs was designed. In [31], comparison of outer and inner rotor SRM was carried out. The efficiency and torque per ampere ratio of outer rotor machine were 92% and 12.8 Nm/A, respectively, and for inner rotor machine in all the cases, they were 90.7% and 12 Nm/A, respectively. The paper showed that the outer rotor machine was suitable for applications requiring high torque density and efficiency. A paper [32] presented the design of a SRM having torque, power, speed-range, and efficiency values competitive to those of the interior IPMSM employed in the 2009 Toyota Prius. The outer diameter and axial length were the same as those of the IPMSM. The simulation results showed that the shaft output power of the SRM enhanced to 1.6 times than the power of the IPMSM at high speed, while its current density and weight were increased by about 15–25%.

1.3. Contribution and proposed approach

We can find numerous studies in literature relevant to SRM design for electric car. However, in the course of designing direct drive motor for EVs, there is no study considering the following factors all together that are aforementioned vehicle dynamics, the constraints including outer diameter and package length of the motor, and five independent variables of motor dimension employed by evolution algorithm even if some of studies exist handling them individually. In this study for the subject EV, a direct drive OR-SRM mounted in wheel is designed and manufactured. Considering vehicle dynamics as designing SRM, optimum design parameters of OR-SRM are estimated by GA to raise efficiency and satisfy the deserved torque. Furthermore, OR-SRM magnetic circuit equations are derived by using seven base flux paths, which are utilized in calculation of motor efficiency and its torque. Nonlinear solution is carried out, involving B-H characteristics of silicon sheet in the equations. The multi-objective optimization problem is solved by accounting some of constraints such as package length, stator outer diameter fitting into the rim, and well-known SRM design considerations. In the present study, multiparameters including stator and rotor pole arc angles, their yoke lengths, and inner diameter of rotor are optimized using objective functions such that the highest efficiency for deserved torque is obtained.

1.4. Layout

Section 2 describes stages of an 18/12 OR-SRM design. Besides, determination of output torque, stator and rotor pole arcs, and calculation of other parameters are comprehensively explained in this section. In Section 3, the analysis of motor via Maxwell 3D software package is carried out. MATLAB analytical solution results are compared to Maxwell 3D results. Experimental results and discussions are provided, and comparison of Maxwell 3D and experimental results are performed in Section 4. Conclusions are given at the end.

2. Preliminaries of the system

In this study, a direct drive motor for EV has been designed and manufactured by using evolutionary algorithm. There are several factors reducing torque ripple of SRMs such as number of phases, pole numbers of stator and rotor, and trigger angle of phases. However, the increasing number of phases causes complexity of control and drive circuit system and also production cost to rise. Motor torque is estimated via specified factors affecting the vehicle performance that are acceleration, aerodynamic forces, and road slope. Specified rim size is selected such that it can fit the motor providing the required torque. And, the voltage and current values are selected considering nominal speed of the vehicle. Furthermore, OR-SRM nonlinear magnetic equations regarding the motor dimension are obtained. Considering the constraints of rim size and OR-SRM base speed, the motor design is performed by genetic algorithm. Eventually, the results of Maxwell 3D software are obtained with the objective of validation. The system diagram of the proposed approach is given in **Figure 1**, and its expansion is provided in the rest of the present section.

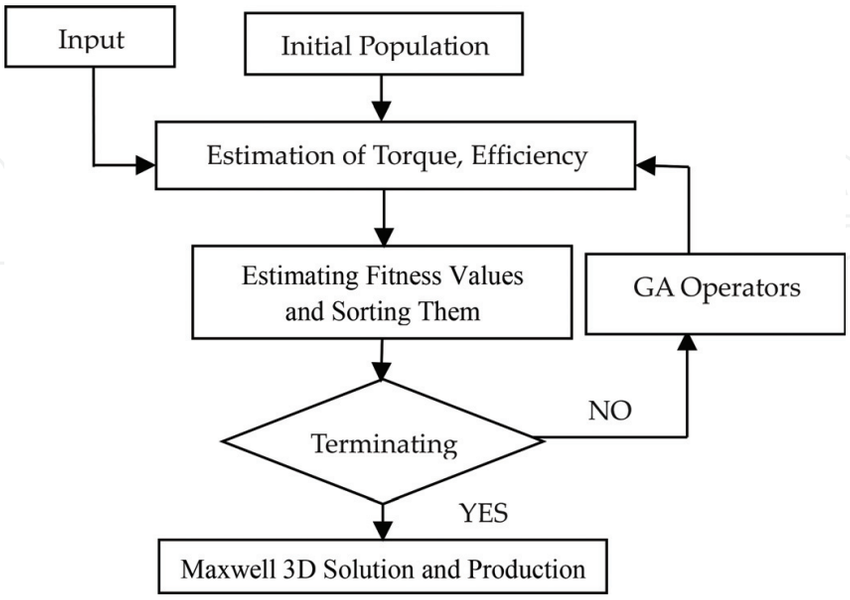

Figure 1. The system diagram of the proposed approach.

http://dx.doi.org/10.5772/intechopen.74451

2.1. Estimation of torque generated by OR-SRM

The electric motors to be manufactured should drive the car to match the following conditions:

1. The EV speed should be up to 120 km/h (aerodynamic force).
2. It should be able to accelerate to 100 km/h in 10 s (aerodynamic and acceleration forces).
3. It should be able to climb 6% slope at 80 km/h constant speed (aerodynamic and slope forces).

When the torque of EV is calculated for three conditions given as above, the highest torque can be obtained in condition 2. If the motors satisfy condition 2, it means that they already satisfy the other conditions. Therefore, the torque estimation should be performed considering condition 2. In this situation, the torque equation can be estimated as

$$T_r = \left(m_v \cdot a_v + \frac{1}{2} \cdot c_w \cdot \delta_a \cdot s_f \cdot v^2 + c_r \cdot m_v \cdot g \right) . r \tag{1}$$

where T_r represents the total torque to be generated by the motor, m_v refers to EV mass, a_v is the acceleration of EV, c_w is aerodynamic coefficient of the EV, δ_a is air density, s_f is perpendicular cross section of the EV, v is the speed of the EV, c_r is the rolling coefficient, g (9.81 m/s^2) is acceleration of gravity, and r is the radius of the EV wheel. These specified EV parameters and estimated torque value for each motor are shown in **Table 1**. Also, the range of EV on a not sloping road which has 90 km/h speed is approximately calculated as 230 km.

2.2. Deriving equations of OR-SRM electric and dimension parameters

Considering the aforementioned number of poles, outer diameter, package size, and air gap, electrical and dimensional parameters are estimated. Dimension parameters of OR-SRM in the equations are shown in **Figure 2**.

B-H characteristic of magnetic sheet plays a crucial role. Therefore, B-H characteristic is considered by catalog data, as seen in **Figure 3**. To put into practice the design of reluctance motor, magnetic induction density is desired not to excess knee point of B-H curve under nominal conditions. Therefore, the following situations are considered by:

1. If pole angle of rotor is greater than that of stator, knee point is taken as maximum rate of magnetic induction density.
2. If pole angle of stator is greater than that of rotor, maximum value of magnetic induction density is specified under knee point, such that avoiding excessive saturation and this value can be obtained considering proportion surface fields of stator and rotor pole.

m_v (kg)	S_f (m^2)	δ_a(m^3/s)	c_w	c_w	r (m)	Estimated torque for each motor (Nm)
1500	1.5	1.255	0.3	0.03	0.37	451.675

Table 1. Specified EV parameters and estimated torque value for each motor.

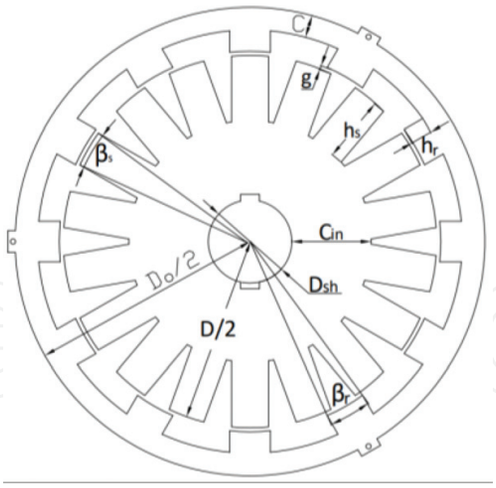

Figure 2. Dimension parameters of OR-SRM.

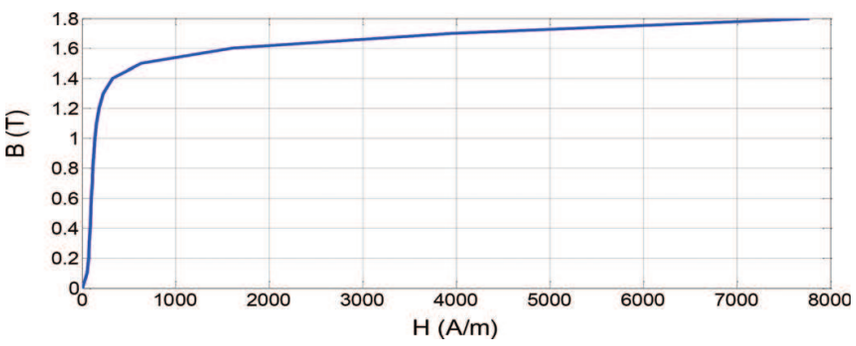

Figure 3. B-H characteristic of M470-50A silicone sheet.

The flux density of stator pole (B_s) is assumed as equal to B_{max}. Omitting leakage flux and packaging factor, stator pole area (A_s) is estimated as

$$A_s = \left(\frac{D}{2} - g\right) \cdot L \cdot \beta_s \tag{2}$$

Flux in stator pole is

$$\varnothing = B_s \cdot A_s \tag{3}$$

Flux in yoke is

$$\varnothing_y = \frac{\varnothing}{2} = \frac{B_s \cdot A_s}{2} \tag{4}$$

Area of yoke is

http://dx.doi.org/10.5772/intechopen.74451

$$A_y = C_{in} \cdot L \tag{5}$$

Flux density of yoke is

$$B_y = \frac{Q_y}{A_y} \tag{6}$$

Length of stator pole is

$$h_s = \left(\frac{D}{2} - g - \frac{D_{sh}}{2}\right) - \frac{A_y}{L} \tag{7}$$

Length of rotor pole is

$$h_r = \frac{D_0}{2} - C - \frac{D}{2} \tag{8}$$

Magnetic field intensity in air gap is calculated by

$$H_g = \frac{B_g}{4 \cdot \pi \cdot 10^{-7}} \tag{9}$$

B-H curve is determined as a function; then, magnetic field density values corresponding to B_s, B_g, B_r, and B_{rc} are obtained by this function. Consequently, the flux path equations are estimated. Thus, path length of rotor region is

$$l_r = h_r + \frac{C}{2} \tag{10}$$

Path length of rotor yoke is

$$l_{ry} = (2 \cdot \pi \cdot NP \cdot 0.5 \cdot (D_0 - C))/N_s \tag{11}$$

where NP refers to the number of phase.

Path length of air gap region is

$$l_g = g \tag{12}$$

Path length of stator region is

$$l_s = (0.25 \cdot D - 0.5 \cdot g + 0.5 \cdot h_s - 0.25 \cdot D_{sh}) \tag{13}$$

Path length of stator core is

$$l_{sy} = (0.5 \cdot (D_{sh} + C_{in}) \cdot 2 \cdot \pi \cdot NP)/N_s \tag{14}$$

In this situation, total ampere-turns can be calculated as

$$TAT = 2 \cdot (H_s \cdot l_s + H_r \cdot l_r) + \left(B_g \cdot \frac{A_g}{P_a}\right) + \left(H_{ry} \cdot l_{ry} + H_{sy} \cdot l_{sy}\right) \tag{15}$$

where P_a refers to permeability.

Turn per phase is

$$T_{ph} = \frac{TAT}{I_p} \tag{16}$$

where I_p refers to rated current.

Current rate is

$$i_p = \frac{TAT}{T_{ph}} \tag{17}$$

Accurate estimation of inductances, L_a and L_u, is crucial for reliable design. High estimation error of inductances causes the torque to be calculated wrong. Therefore, to calculate the inductances (L_a and L_u) at aligned and unaligned positions, respectively, 2 base and 7 base flux paths are selected. The rest of the fluxes can cause rising of the estimation complexity, and variation of the result will be trivial, as shown in **Figures 4** and **5**.

Tube 1 and Tube 7 flux paths are employed to calculate L_a. Eqs. (13) and (14) calculate ampere-turns of Tube 1 and Tube 7, namely. Eq. (15) estimates the inductance at aligned position. Eq. (17) refers to calculation of leakage inductance in Tube 7. Herein, B_{smin} is the value equalizing Eq. (14) to Eq. (16). Consequently, Equation (18) calculates the inductance of a single pole pair at aligned position:

$$TAT_1 = 2 \cdot (H_s \cdot l_s + H_r \cdot l_r) + \left(B_g \cdot \frac{A_g}{P_a}\right) + \left(H_{ry} \cdot l_{ry} + H_{sy} \cdot l_{sy}\right) \tag{18}$$

$$TAT\_7 = H_s \cdot l_s + \frac{B_s \cdot A_{sf}}{P_f} + H_{sy} \cdot l_{sy} \tag{19}$$

$$L_1 = TAT\_1 \cdot \frac{B_s \cdot A_s}{i_p^2} \tag{20}$$

$$TAT_7 = \left(\frac{3}{4}\right) \cdot \frac{1}{2} \cdot T_{ph} \cdot i \tag{21}$$

$$L_7 = TAT\_7 \cdot \frac{B_{smin} \cdot A_{sf}}{i_p^2} \tag{22}$$

http://dx.doi.org/10.5772/intechopen.74451

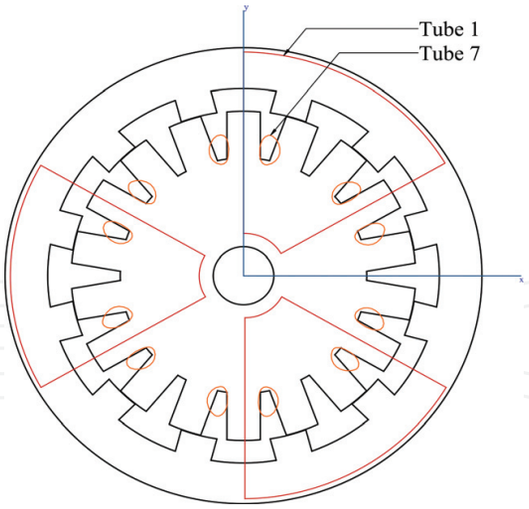

Figure 4. Flux paths for inductance calculation of OR-SRM at aligned position (L_a).

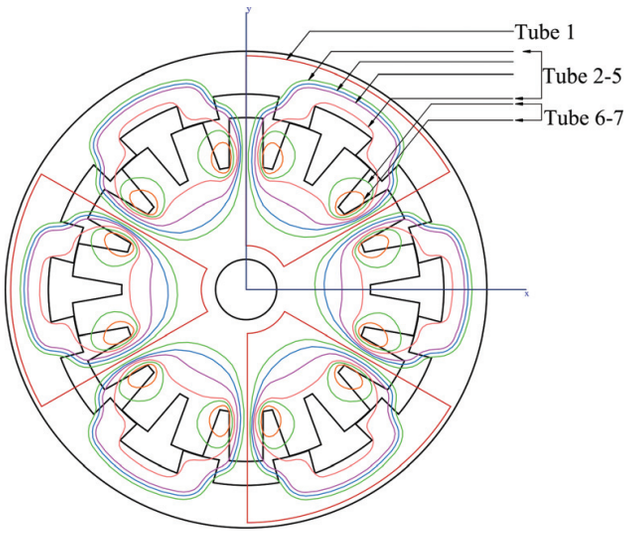

Figure 5. Flux paths for inductance calculation of OR-SRM at unaligned position (L_u).

$$L_a = L_1 + 4 \cdot L_7 \tag{23}$$

At this stage, the aligned inductance for a single phase is obtained by

$$L_{a\_phase} = N_{tpp} \cdot 0.5 \cdot L_a \tag{24}$$

where N_{tpp} represents the number of teeth per phase.

The flux paths in **Figure 5** estimate L_u for a single pole pair. Equations (20)–(23) calculate total ampere-turns of each flux path. Substituting B_{smin} into Eq. (24), inductance of its own flux path is obtained:

$$TAT_1 = T_{ph}\cdot i = 2\cdot(H_s\cdot l_s) + \frac{B_s\cdot A_{1s}}{P_1} + \frac{H_{sy}\cdot l_{sy}}{2} + \frac{H_g.l_g}{2} \tag{25}$$

$$TAT_n = 2\cdot(H_{sn}\cdot l_{sn} + H_{rn}\cdot l_{rn}) + \frac{B_{sn}\cdot A_{sn}}{P_n} + \ldots\left(H_{ryn}\cdot l_{ryn} + H_{syn}\cdot l_{syn}\right)(n = 2,3,4,5) \tag{26}$$

$$TAT_6 = \left(\frac{1}{2}\right)\cdot\frac{5\cdot T_{ph}\cdot i}{4} = 2\cdot H_s\cdot l_s + \frac{B_s\cdot A_{6s}}{P_6} + H_{sy}\cdot l_{sy} \tag{27}$$

$$TAT_7 = \frac{T_{ph}\cdot i}{4} = H_s\cdot l_s + \frac{B_s\cdot A_{7s}}{P_7} + H_{sy}\cdot l_{sy} \tag{28}$$

$$L_{u(k)} = TAT_{(k)}\cdot\frac{B_{smin(k)}\cdot A_{(k)s}}{{i_p}^2}\ (k = 1,2,3,4,5,6,7) \tag{29}$$

Finally, inductance of a single pole pair at unaligned position is calculated by

$$L_u = L_{u1} + 2\cdot(L_{u2} + L_{u3} + L_{u4} + L_{u5}) + 4\cdot(L_{u6} + L_{u7}) \tag{30}$$

At this stage, the unaligned inductance for a single phase is obtained by

$$L_{u\_phase} = N_{tpp}\cdot 0.5\cdot L_u \tag{31}$$

Energy calculation at aligned and unaligned position, average torque of pole pair, and average torque are all, respectively, given as

$$W_a = \frac{1}{2}\cdot L_a\cdot {i_p}^2 \tag{32}$$

$$W_u = \frac{1}{2}\cdot L_u\cdot {i_p}^2 \tag{33}$$

$$T_{pp} = \frac{((W_a - W_u)\cdot N_s\cdot N_r)}{N_{tpp}\cdot\pi} \tag{34}$$

$$T_{average} = T_{pp}\cdot N_{tpp}\cdot 0.5 \tag{35}$$

The coil length of pole pair is obtained by

$$l_{pp} = 4\cdot\left[L + \left(\frac{(0.5\cdot D - g - 0.5\cdot h_s)\cdot 2\cdot\pi}{18}\right)\right]\cdot T_{ph} \tag{36}$$

Conductor area of conductor diameter (0.95) is given as

$$CA = (0.95)^2\cdot 0.25\cdot\pi\cdot NR \tag{37}$$

where NR refers to the number of wires.

Pole and phase resistances are, respectively, estimated by

http://dx.doi.org/10.5772/intechopen.74451

$$R_{s1} = \left(0.0177 \cdot I_{pp}\right)/CA \tag{38}$$

$$R_s = N_{tpp} \cdot 0.5 \cdot R_{s1} \tag{39}$$

Copper loss is calculated in

$$P_{cl} = \left(I_p\right)^2 \cdot R_s \tag{40}$$

And, iron volume is provided as

$$D_{vol} = \left[\left((A_s \cdot h_s \cdot N_s) + (A_r \cdot h_r \cdot N_r)\right) + \pi \cdot L \cdot \left((0.5 \cdot D - g - h_s)^2 + (0.5 \cdot D_0)^2 - (0.5 \cdot D_0 - C)^2\right)\right] - V_{cool} \tag{41}$$

where V_{cool} is the total volume of the cooling holes.

Torque/volume rate is given in

$$TVolume = T_{average}/D_{vol} \tag{42}$$

Efficiency is obtained by

$$\eta(\%) = ((P_i - P_{cl})/P_i) \cdot 100 \tag{43}$$

2.3. Optimization of motor dimension parameters using genetic algorithm

Calculation of dimension parameters for SRM could be optimized by trial and error, but estimated cost of these types of methods is fairly high. And also, convergence could not be manually accomplished in every experiment including specified trials. Because tiny tuning inputs on the dimension parameters can emerge large variations on the motor torque and its efficiency.

Exploring optimum values of five different parameters, $f_{\text{obj}}(\beta_s, \beta_r, D, C_{in}, C)$, to be involved in the object functions is NP-complete problem. Therefore, evolutionary algorithm is proposed to solve NP-complete combinatorial optimization problems. Genetic approach generates better individuals influencing torque and efficiency for each new generation. Stages of the proposed GA are given by:

2.3.1. Coding individuals

Thirty-two-bit binary codes for each individual are utilized to build genes. Each of parameters, β_s, β_r, D, C_{in}, and C are represented by five bits, all of them stands for chromosome.

The restrictions of the optimized parameters are taken into consideration as below [33]:

- Rotor pole arc is selected to be equal or greater than stator pole arc, since the number of rotor pole is less than the number of stator pole.

- βs should be equal or greater than step angle to generate required torque using OR-SRM. When βs is selected as smaller than step angle, none of the phases may not have rising inductance slope.
- Rotor pole angle should be greater than the sum of stator and rotor pole arc.
- Other parameters such as magnetic saturation and physical strength are also considered in these restrictions.

We have used 25 bits out of 32 bits as shown in **Figure 6**. Out of range values are not included in the solution space. The constraints with regard to motor dimension parameters are also involved in fitness function to reduce solution space, which are given as.

$$\beta_s + \beta_r < \left(\frac{360}{N_r}\right), \beta_s \le \beta_r, \text{torque} > 400$$

$$80 < \textit{efficiency} < 100, 0.4 < \beta_r - \beta_s < 1.8$$

$$11 \le \beta_s \le 15, 12 \le \beta_r \le 16, 0.160 \le D \le 0.185$$

$$0.012 \le C \le 0.032, 0.06 \le C_{in} \le 0.091, 0 \le P \le \left(2^{25} - 1\right)$$

Considering constraints above, five bits of D, C, C_{in}, β_r, and β_s are sufficient to get a result in required precision.

2.3.2. Initial population

The population consists of n individuals each of which includes aforementioned five parameters. n is taken as 200. Allowing the entire range of possible solutions, they are randomly produced by

$$P = \text{int}\left(\text{rand}(\,) \cdot \left(2^{25} - 1\right)\right) \tag{44}$$

2.3.3. Generating offspring

The fitness function is defined by considering required torque and efficiency that are, respectively, 450–500 Nm and over 80%.

Estimation of fitness rate: Fitness function is designated by required torque and efficiency of motor as

NULL	C_{in}	C	D	β_r	β_s
31. - - - - - - -	- - - - -	- - - - -	- - - - -	- - - - -	- - - - - 0.

Figure 6. Chromosome of each individual.

$$fitness = \left(\left(\frac{Torque}{400}\right) + \left(\frac{efficiency}{100}\right)\right) \cdot 100 \tag{45}$$

The individuals are sorted in fitness values. Then, the individuals, whose the fitness values are better, remain in the population, and the ones whose fitness values are worse are eliminated. Therefore, in each iteration, quarter of the population turns out to be eliminated. Sorted population is shown in **Figure 7**.

Crossover operator: Random 2 bits out of least significant 25 bits of parents are crossed to generate a new offspring couple. The chromosome of parents and offspring are given in **Figure 8(a)** and **(b)**.

Mutation operators: Mutation rate is specified as 0.05 to reach global solution.

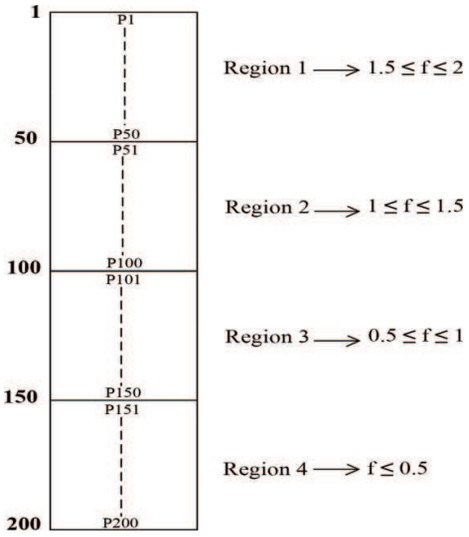

Figure 7. Sorted population.

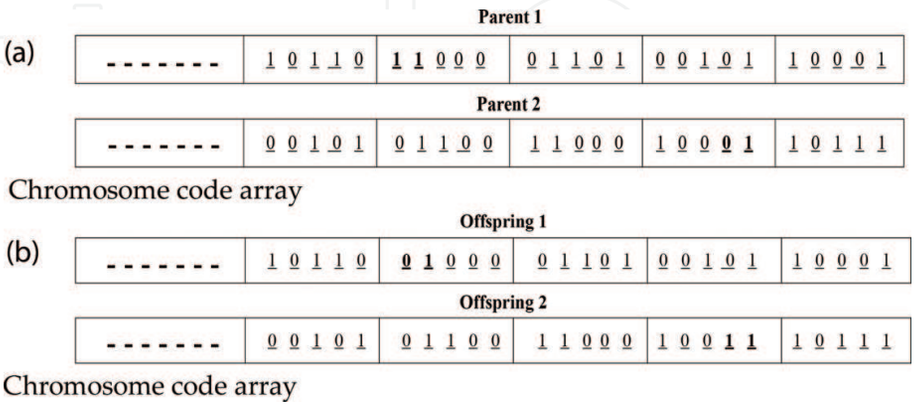

Figure 8. (a) Chromosome of parents, (b) Chromosome of offspring.

Optimized parameters					The other dimension parameters			Electrical parameters			Fitness	
β_r (deg.)	β_s (deg.)	D (mm)	C (mm)	C_{in} (mm)	h_s (mm)	h_r (mm)	D_{sh} (mm)	R_f (Ω)	L_u (mH)	L_a (mH)	T (Nm)	η (%)
12.26	11.13	182.7	21.7	76	66.2	20.6	80	0.33	6.4	20.7	467.72	93.69

Table 2. Estimated parameters for the manufactured OR-SRM.

2.3.4. Termination criteria

The derivation of the fitness values is calculated by

$$\varepsilon = \sum_{i=1}^{n/2} \left(f_i - f_{i-1}\right) \tag{46}$$

Here, termination criteria are determined as $\varepsilon \leq 0.001$.

Considering fitness constraints, optimized values of five parameters, correspondent motor dimension, and electrical parameters are given in **Table 2**.

3. The analysis of motor using Maxwell 3D package software

To validate OR-SRM design parameters, Maxwell 3D analysis is carried out following manufacturing stage. Field distribution, inductance, and torque curves are consecutively plotted by Maxwell 3D software as shown in **Figures 9–11**. MATLAB analytical solution results are verified with Maxwell 3D results as given in **Table 3**.

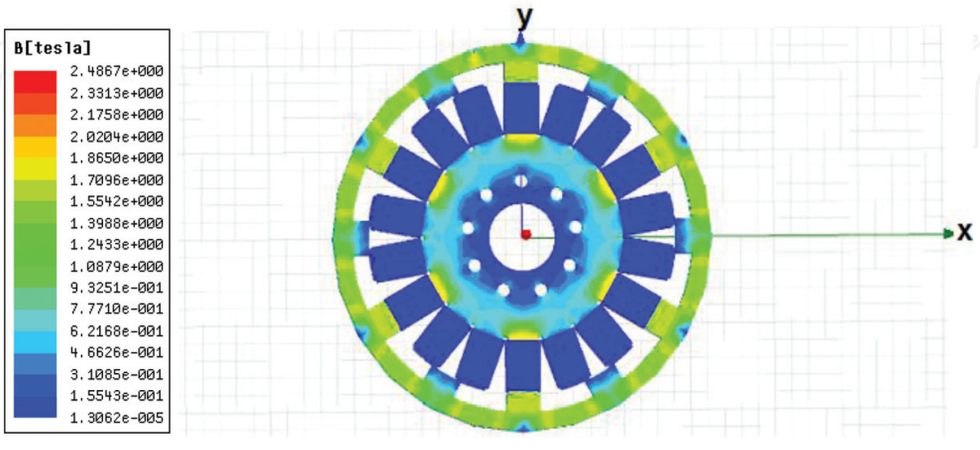

Figure 9. Field distribution of 18/12 OR-SRM.

http://dx.doi.org/10.5772/intechopen.74451

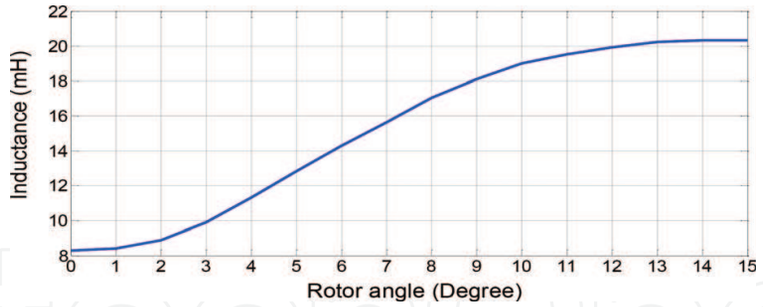

Figure 10. Inductance curve of 18/12 OR-SRM.

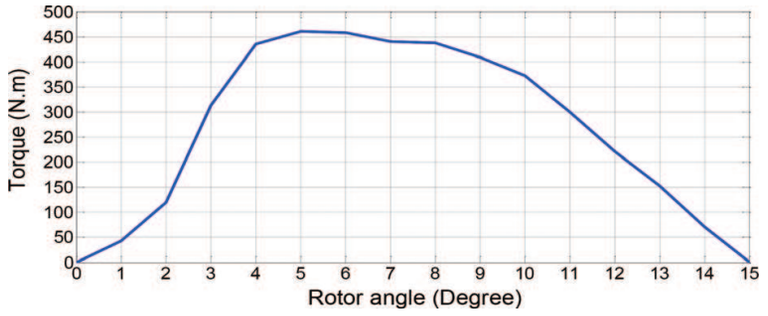

Figure 11. Torque curve of 18/12 OR-SRM.

	GA Solution	Maxwell 3D	Error %
Torque (Nm)	467.72	460.47	1.57
Efficiency (%)	93.69	95.28	1.6

Table 3. Comparison of GA solution and Maxwell 3D results.

4. Experimental results and discussions

OR-SRM has been manufactured by using motor sizes optimized via MOGA. The motor at manufacturing stage is given in **Figure 12**. OR-SRM is cooled via cooling channels shown in **Figure 12** as the forced circulation air cooling. A nematic air dryer compressor is used to cool the OR-SRM. Thus, the temperature of the motor is prevented by these cooling channels to reach too high levels. Therefore, the changes in the winding resistance are minimized. Its negative effect on the efficiency is also reduced.

The manufactured OR-SRM is shown in **Figure 13**.

In this study, asymmetric half-bridge converter is designed and used to feed OR-SRM. A capacitor charged and discharged by switching IGBT is connected between the battery and

Figure 12. Stator windings of OR-SRM at manufacturing stage.

Figure 13. Manufactured OR-SRM.

converter. According to different speeds and reference currents, trigger angles of each phase winding are calculated. The trigger angles are correlated to the speed, battery voltage, reference current, and rotor position.

To compare the estimated torque obtained by Maxwell 3D and that of the manufactured motor, locked rotor experiment has been carried out. Herein, torque rate is measured by torque sensor mounted on tested while streaming the coil current, 75 A by locking OR-SRM rotor at designated positions.

Test bed of OR-SRM is shown in **Figure 14**. OR-SRM is loaded with an induction motor controlled by the direct torque control driver. Torque sensor is used for measuring torque of OR-SRM. The features of torque sensor have very short construction, broad input voltage range, current, and output voltage; the measurement accuracy is less than 0.5% of full scale; and measurement ranges change from 5 to 500 Nm. The control algorithm is run by dSPACE DS1103. Hall-effect current and voltage sensors are used for measuring motor phase and battery currents and battery voltage.

The comparison of Maxwell 3D and experimental results have been drawn in **Figure 15**.

Average rate of relative errors between Maxwell 3D and experimental results is estimated as 2.248%, for the angles at designated positions.

http://dx.doi.org/10.5772/intechopen.74451

Figure 14. OR-SRM test bed.

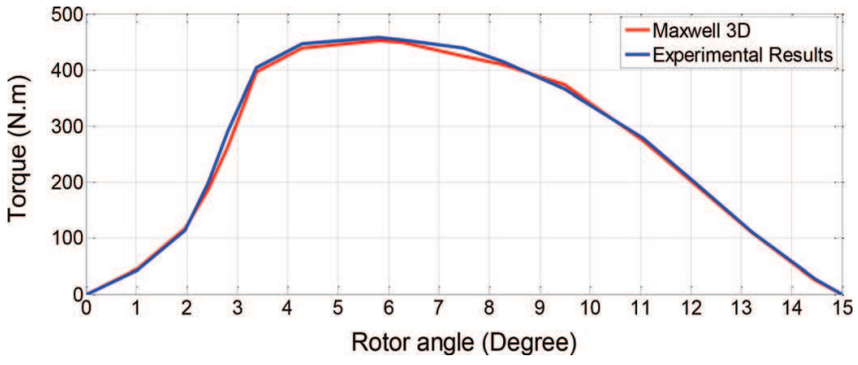

Figure 15. Comparison of Maxwell 3D and experimental results.

In this paper, we have proposed an optimum solution satisfying the torque and efficiency of OR-SRM via MOGA considering constrains of EV dynamics. The efficiency and torque values are the components of objective function. Torque density has not been involved in the objective function since the package length and outer diameter are specified to fit into 21-inch wheel rim. The solution of torque ripple problem might be considered by varying trigger angles in motor control stage rather involving it during OR-SRM design stage, which is well-known motor control method. As a future work, torque ripple will be involved in multi-objective optimization function via analysis of dynamic solution.

5. Conclusion

In this study, a direct drive OR-SRM mounted in wheel is designed and manufactured for the subject EV. The dimensional and electrical parameters of 18/12 OR-SRM for EV have been calculated by multi-objective evolutionary algorithm. The mathematical equations derived by geometry of OR-SRM have been used to get results from objective functions resided in fitness

function. The vehicle dynamics, five independent variables of motor dimension, and the constraints including outer diameter and package length of the motor are employed by evolution algorithm. The multiparameters including stator and rotor pole arc angles, their yoke lengths, and inner diameter of rotor are optimized using objective functions such that the highest efficiency for deserved torque is obtained. Consequently, we can obviously suggest that this approach could be conducted to design a standard-type OR-SRM.

Acknowledgements

The authors gratefully acknowledge the support of the Scientific and Technological Research Council of Turkey (No: 113 M090).

Author details

Zeki Omaç[1], Mehmet Polat[2], Mustafa Kaya[3], Eyyüp Öksüztepe[4], Haluk Eren[4]*, Merve Yıldırım[5] and Hasan Kürüm[5]

*Address all correspondence to: he.edu.tr@gmail.com

1 Electrical and Electronics Engineering, University of Munzur, Tunceli, Turkey

2 Mechatronics Engineering, University of Fırat, Elazığ, Turkey

3 Digital Forensics Engineering, University of Fırat, Elazığ, Turkey

4 School of Aviation, University of Fırat, Elazığ, Turkey

5 Electrical and Electronics Engineering, University of Fırat, Elazığ, Turkey

References

[1] Yildirim M, Polat M, Kürüm H. A survey on comparison of electric motor types and drives used for electric vehicles. In: IEEE 16th International Power Electronics and Motion Control Conference and Exposition (PEMC); 2014. pp. 218-223

[2] Trancho E, Ibarra E, Arias A, Kortabarria I, Prieto P. A practical approach to HFI based sensorless control of PM-assisted synchronous reluctance machines applied to EVs and HEVs. In: IEEE 43rd Annual Conference of the Industrial Electronics Society (IECON); 2017. pp. 1735-1740

[3] Tarek MTB, Choi S. Design and rotor shape modification of a multiphase high speed permanent magnet assisted synchronous reluctance motor for stress reduction. In: IEEE Energy Conversion Congress and Exposition (ECCE); 2007. pp. 5389-5395

[4] Asgar M, Afjei E, Behbahani A, Siadatan A. A 12/8 double-stator switched reluctance motor for washing machine application. In: IEEE 6th Power Electronics, Drives Systems & Technologies Conference (PEDSTC); 2015. pp. 168-172

[5] Tursini M, Villani M, Fabri G, Di Leonardo L. A switched-reluctance motor for aerospace application: Design, analysis and results. Electric Power Systems Research. 2017; **142**:74-83

[6] Öksüztepe E. In-wheel switched reluctance motor design for electric vehicles by using a pareto-based multiobjective differential evolution algorithm. IEEE Transactions on Vehicular Technology. 2017;**66**(6):4706-4715

[7] Santiago JD, Bernhoff H, Ekergard B, Eriksson S, Ferhatovic S, Waters R, Leijon M. Electrical motor drivelines in commercial all-electric vehicles: A review. IEEE Transactions on Vehicular Technology. 2012;**61**(2):475-484

[8] Xue XD, Cheng KWE, Cheung NC. Selection of electric motor drivers for electrical vehicles. In: IEEE Power Engineering Conference, AUPEC'08; Australasian Universities; 2008. pp. 1-6

[9] Wenping C, Mecrow BC, Atkinson GJ, Bennett JW, Atkinson DJ. Overview of electric motor technologies used for more electric aircraft (MEA). IEEE Transactions on Industrial Electronics. 2012;**59**(9):3523-3531

[10] Rahman KM, Fahimi B, Suresh G, Rajarathnam AV, Ehsani M. Advantages of switched reluctance motor applications to EV and HEV: Design and control issues. IEEE Transactions on Industry Applications. 2000;**36**(1):111-121

[11] Ramu K. Switched Reluctance Motor Drives: Modeling, Simulation, Analysis, Design, and Applications. U.S.: CRC Press, Taylor and Francis Group; Dec, 2017

[12] Miller TJE. Electronic Control of Switched Reluctance Machines. U.S.: Elsevier, Newnes; 2001

[13] Yildirim M, Polat M, Oksuztepe E, Omac Z, Yakut O, Eren H, Kaya M, Kurum H. Designing in-wheel switched reluctance motor for electric vehicles. In: IEEE 16th International Power Electronics and Motion Control Conference and Exposition (PEMC); 2014. pp. 793-798

[14] Sengor I, Polat A, Ergene LT. Design and analysis of switched reluctance motors. In: IEEE 8th International Conference on Electrical and Electronics Engineering (ELECO); Nov. 2013. pp. 586-590

[15] Sakthivel P, Chandrasekar V, Arumugam R. Design of a 250w, low speed switched reluctance hub motor for two wheelers. In: IEEE 1st International Conference on Electrical Energy Systems (ICEES); Jan. 2011. pp. 176-181

[16] Koibuchi K, Ohno T, Sawa K. A basic study for optimal design of switched reluctance motor by finite element method. IEEE Transactions on Magnetics. 1997;**33**(2):2077-2080

[17] Jawad F, Shahgholian G, Ghazizadeh H. Analysis of dynamic behavior of switched reluctance motor-design parameters effects. In: IEEE 15th Mediterranean Electrotechnical Conference; 2010. pp. 532-537

[18] Takano Y, Takeno M, Hoshi N, Chiba A, Takemoto M, Ogasawara S, Rahman MA. Design and analysis of a switched reluctance motor for next generation hybrid vehicle without PM materials. In: IEEE International Power Electronics Conference (IPEC); June 2010. pp. 1801-1806

[19] Chiba A, Takano Y, Takeno M, Imakawa T, Hoshi N, Takemoto M, Ogasawara S. Torque density and efficiency improvements of a switched reluctance motor without rare-earth material for hybrid vehicles. IEEE Transactions on Industry Applications. 2011;**47**(3): 1240-1246

[20] Mirzaeian B, Moallem M, Tahani V, Lucas C. Multiobjective optimization method based on a genetic algorithm for switched reluctance motor design. IEEE Transactions on Magnetics. 2002;**38**(3):1524-1527

[21] Yoshiaki K, Kosaka T, Matsui N. Optimum design approach for a two-phase switched reluctance compressor drive. IEEE Transactions on Industry Applications. 2010;**46**(3): 955-964

[22] Omekanda AM. Robust torque and torque-per-inertia optimization of a switched reluctance motor using the Taguchi methods. IEEE Transactions on Industry Applications. 2006;**42**(2):473-478

[23] Cosovic M, Smaka S, Salihbegovic I, Masic S. Design optimization of 8/14 switched reluctance machine for electric vehicle. In: IEEE XXth International Conference on Electrical Machines (ICEM); 2012. pp. 2654-2659

[24] Naayagi MR, Kamaraj V. Optimal design of switched reluctance machine using genetic algorithm. Optimization. 2002;**19**(1):350-353

[25] Behzad MD, Moallem P. Genetic algorithm based optimal design of switching circuit parameters for a switched reluctance motor drive. In: IEEE International Conference on Power Electronics, Drives and Energy Systems (PEDES); 2006

[26] Costa MC, Nabeta SI, Dietrich AB, Cardoso JR, Marechal Y, Coulomb JL. Optimisation of a switched reluctance motor using experimental design method and diffuse elements response surface. IEE Proceedings - Science, Measurement and Technology. 2004;**151**(6): 411-413

[27] Zhang Y, Xia B, Xie D, Koh CS. Optimum design of switched reluctance motor to minimize torque ripple using ordinary Kriging model and genetic algorithm. In: IEEE International Conference onElectrical Machines and Systems (ICEMS); Aug. 2011. pp. 1-4

[28] Ma C, Qu L. Multiobjective optimization of switched reluctance motors based on design of experiments and Particle Swarm Optimization. In: IEEE Transactions on Energy Conversion. 2015;(**30**)3:1144-1153

[29] Labak A, Narayan CK. Outer rotor switched reluctance motor design for in-wheel drive of electric bus applications. In: IEEE XXth International Conference on Electrical Machines (ICEM); 2012

[30] Xue XD, Cheng KWE, Ng TW, Cheung NC. Multi-objective optimization design of in-wheel switched reluctance motors in electric vehicles. IEEE Transactions on Industrial Electronics. 2010;**57**(9):2980-2987

[31] Hennen MD, Rik WDD. Comparison of outer-and inner-rotor switched reluctance machines. In: IEEE 7th International Conference on Power Electronics and Drive Systems (PEDS); 2007

[32] Kiyota K, Akira C. Design of switched reluctance motor competitive to 60-kW IPMSM in third-generation hybrid electric vehicle. IEEE Transactions on Industry Applications. 2012;**48**(6):2303-2309

[33] Omaç Z, Polat M, Öksüztepe E, Yıldırım M, Yakut O, Eren H, Kaya M, Kürüm H. Design, analysis, and control of in-wheel switched reluctance motor for electric vehicles. Electrical Engineering

IntechOpen